Effects of clay content on the volumetric behavior of loess under heating-cooling cycles[*]

Qing-yi MU[1], Charles Wang-wai NG[2], Chao ZHOU[†‡3], Gordon Gong-dan ZHOU[4]

[1]*Department of Civil Engineering, Xi'an Jiaotong University, Xi'an 710049, China*

[2]*Department of Civil and Environmental Engineering, The Hong Kong University of Science and Technology, Hong Kong 999077, China*

[3]*Department of Civil and Environmental Engineering, The Hong Kong Polytechnic University, Hong Kong 999077, China*

[4]*Key Laboratory of Mountain Hazards and Earth Surface Process, Chinese Academy of Sciences (CAS), Chengdu 610041, China*

[†]E-mail: c.zhou@polyu.edu.hk

[‡] Corresponding author

ⓘ ORCID: Qing-yi MU, https://orcid.org/0000-0002-9235-4978; Chao ZHOU, https://orcid.org/0000-0002-9443-6707

Abstract: Although numerous studies have been carried out on investigating thermal volume changes in different soils, limited attention has been paid to loess. This study aims to investigate the effects of clay content on the deformation of loess under heating-cooling cycles. Three soils with different clay contents (i.e. SA: 7%; SB: 13%; SC: 35%) were prepared with loess collected in situ through the sedimentation method. The soil volume changes were measured under heating-cooling cycles by using a thermal invar oedometer. To interpret the experimental results, X-ray diffraction (XRD) and scanning electron microscope (SEM) tests were conducted to identify the composition and microstructure of tested soils, respectively. The results show that the plastic axial strains of SA, SB, and SC accumulate to a certain level with the increasing number of heating-cooling cycles. At the stable state, the plastic axial strain of SC is 264% and

52% larger than those of SA and SB, respectively. On the other hand, the linear thermal expansion coefficient of SC is 66% and 20% larger than those of SA and SB, respectively. As evidenced from the XRD test, the clay in loess mainly contains kaolinite, chlorite, and illite, while the composition of silt is dominated by quartz. The clay minerals are more sensitive to thermal fluctuations than quartz because of the electrical double layer. SC, whose clay content is deliberately enhanced, exhibits a larger plastic axial strain and linear thermal expansion coefficient than do SA and SB.

Key words: Loess; Volumetric behavior; Clay mineral; Heating-cooling cycles

1 Introduction

Loess is widely used as the earthen final cover of landfills in northwestern China (Lu et al., 2015; Zhan et al., 2016). As illustrated in Fig. 1, the final cover mainly consists of a vegetation layer and a compacted loess layer. As one of the important components of waste disposal, the final cover system plays an important role in minimizing percolation into the underlying waste and limiting the emission of landfill gas (Zhan et al., 2017; Ng et al., 2019b). In the field, temperatures within earthen final covers vary in a wide range. According to previous studies (Dach and Jager, 1995; Liu XC et al., 2016), the soil temperature in an earthen final cover could increase to approximately 70 °C due to the heat generated by the waste decomposition. On the other hand, as a typical semi-arid climate region, the atmospheric temperature in northwestern China varies from subzero to several dozen degrees Celsius. The earthen final covers exposed in such a climate will be daily and seasonally heated or cooled. Loess in northwestern China is susceptible to cracking because of its fine contents (Tu et al., 2009; Wang et al., 2014). During heating-cooling, desiccation causes the loss of soil water to the atmosphere and the subsequent cracking of the loess, consequently lowering the barrier's efficiency in preventing water infiltration and gas emission (Southen and Rowe, 2005; Zhan et al., 2016, 2017; van Dijk, 2018). Based on field tests, Zhan et al. (2017) observed drying-induced cracks in the compacted loess final cover, which resulted in a large amount of water infiltration. Understanding the thermal volume change behavior of the soil is a prerequisite to analyzing the crack formation in earthen final covers induced by heating-cooling.

Thermal volume changes in different soils have been extensively studied from both the theoretical and experimental viewpoints. To improve the serviceability design of repositories for radioactive waste disposal, the heating-induced volume change behavior of expansive clays was widely investigated (Delage et al., 2000; Cekerevac and Laloui, 2004; Abuel-Naga et al., 2007). Heating-induced plastic contraction was observed for normally consolidated and lightly over-consolidated soils. As suggested by Campanella and Mitchell (1968), the expansion of water in the electrical double layer leads to the reconfiguration of the soil structure and hence contraction under externally applied stresses. During thermal loading, the reconfiguration of the soil structure occurs not only in structural soils (e.g. quick clay and natural loess) but also in reconstituted soils (Cekerevac and Laloui, 2004; Ng et al., 2019a). For heavily over-consolidated soils, the

heating process induced an elastic thermal expansion. To understand the deformation behavior of clay under heating-cooling cycles, Campanella and Mitchell (1968) tested normally consolidated illite. Their results showed that the plastic contraction of illite accumulated with the increasing number of heating-cooling cycles. Within approximately three heating-cooling cycles, the contraction of soil specimens reached a stable state, at which point the soil volume changes under heating-cooling cycles were almost elastic. Di Donna and Laloui (2015) studied the volume changes in saturated silty clay under heating-cooling cycles using a thermal oedometer. Similar tests were also carried out by Vega and McCartney (2015) with "Bonny silt". Their results confirmed that the thermally induced soil contraction accumulated with an increasing number of heating-cooling cycles when the soils have low over-consolidation ratio values. Recently, Ng et al. (2019a) investigated the volume change in loess under heating-cooling cycles through thermal oedometer tests. Similar to other soils, the accumulation of plastic contraction was observed for loess under heating-cooling cycles. Furthermore, a qualitative micro-structural analysis using a scanning electron microscope (SEM) showed that the thermal volume changes in loess were significantly influenced by the distribution of clay particles. However, quantitative investigations on the role of clay particles in the thermal deformation of loess were not included in the above study. An insight into the underlying mechanisms in the volume change of loess under heating-cooling cycles is still incomplete.

In the present work, the effects of clay content on the volumetric behavior of loess under heating-cooling cycles were studied through a series of thermal oedometer tests. Based on loess collected in situ (SB sample), the clay mineral content is reduced in the SA sample and enhanced in the SC sample through a sedimentation method. The measured axial strains of these three soils under heating-cooling cycles were analyzed and compared to highlight the effects of clay particles on the thermal volume change of loess. To assist in the interpretation of the test results, X-ray diffraction (XRD) and SEM tests were also carried out to identify the mineral components and microstructure of the tested soils, respectively. It should be noted that the soil volume change depends on the phase change between ice and water at sub-zero temperatures that falls into the category of frozen soil mechanics (Konrad, 1990; Mu et al., 2019). This study aims to investigate the heating-cooling (25–65 °C) induced volume change of loess at above 0 °C.

2 Test apparatus

Fig. 2 illustrates the schematic diagram of the thermal oedometer. The apparatus consists of a conventional oedometer cell, insulation material, and a system for controlling soil temperature. For the conventional oedometer cell, the oedometer ring containing the soil specimen was altered from steel to invar (Ng et al., 2017a). The thermal expansion coefficient of steel ($1.5{\times}10^{-6}$ °C^{-1}) is approximately 30 times larger than that of invar ($5{\times}10^{-7}$ °C^{-1}). Therefore, the invar was utilized to minimize the thermal deformation of the oedometer ring during the heating-cooling tests. A strain gauge with an accuracy of 0.025% was attached to the loading rod. With the movement of the loading rod during mechanical and thermal loadings, the vertical displacement of the soil was recorded. During mechanical loading, the pre-calculated dead weight was added on the loading rod to control the effective vertical stress of the soil specimen. During

the tests, the valves at the bottom of the chamber were closed, letting the water drain only through the top porous stone. The water level was expected to be constant because no water was allowed to flow in or out of the oedometer cell. The heating system consists of a thermostat, a thermocouple, and a heater. Both the heater and the thermocouple were submerged in water. During heating-cooling, the heat output was adjusted by the thermostat according to the feedback of the thermocouple, and the soil specimen was maintained at the predefined temperatures. More information about the heating system is given by Ng et al. (2017b). In addition, the oedometer cell was insulated with foam board to reduce the heat exchange between the oedometer cell and the environment. At a thermal equilibrium state, the temperature fluctuation in the soil sample was less than 0.3 °C. It should be noted that the soil temperature was recorded through the thermocouple attached to the oedometer ring (Fig. 2). According to the calibration tests, the soil temperature next to the oedometer ring was similar to that at the center of the specimen after 5 h for each heating-cooling stage.

The measurement of soil deformation should be corrected by eliminating the apparent deformation of the thermal oedometer. Heating-cooling tests on an aluminum block (of height 50 mm and diameter 70 mm) were carried out to calibrate the apparent deformation of the apparatus. The aluminum block used in the calibration test has a well-defined thermal expansion coefficient (2.3×10^{-5} °C^{-1}) and Young's modulus (69 GPa). The deformation in the aluminum block induced by thermal and mechanical loadings could be eliminated from the measured total deformation to achieve the value of the thermal oedometer. Other materials having a clear thermal expansion coefficient and elastic modulus, such as steel and invar, could also be used for calibration tests. As shown in Fig. 3, the aluminum block exhibits an apparent heave during the first heating process and an apparent settlement during the subsequent cooling process. There is an irreversible axial strain of 0.17% for the thermal oedometer after the first heating-cooling cycle. During the second heating-cooling cycle, the aluminum block shows almost elastic behavior, with an irreversible deformation less than 0.03%. The calibrated apparent deformation is attributed to the thermal response of different components of the apparatus, e.g. steel chamber, loading rod, and porous stone. Similar evolutions in apparent deformations with thermal loading were observed by Ng et al. (2019a) for the calibration of a temperature-controlled oedometer under cyclic heating-cooling. For the subsequent analysis of experimental data, the measured soil deformation during the first heating-cooling cycle was corrected by eliminating the apparent deformation calibrated for this cycle. For the subsequent heating-cooling cycles, all the measured soil deformations were corrected by eliminating the calibration results at the second heating-cooling cycle.

3 Physical properties of the tested loess

Three different soils referred to as SA, SB, and SC were tested in this study. A loess referred to as SB was taken from Xi'an, China. The particle size distribution of the tested loess was measured by both the sieving and sedimentation methods following the procedures proposed by ASTM D422-63 (ASTM, 2007). During sieving, all soil particles passed through a 0.1 mm aperture sieve after gentle grinding. As shown in Fig. 4, for SB, the gravimetric percentages of soil particles ranging from 0.063 mm to 2 mm (sand), 0.002 mm to 0.063 mm (silt),

and smaller than 0.002 mm (clay) are 2%, 85%, and 13%, respectively. SB has a liquid limit of 36% and a plastic limit of 16%. Based on ASTM D2487-11 (ASTM, 2011), SB falls into the category of a clay of low plasticity (CL).

Based on the loess (i.e. SB) collected in situ, two other soils referred to as SA and SC were prepared. SA was prepared by eliminating clay particles from SB through the sedimentation method proposed in ASTM D422-63 (ASTM, 2007). The working principle of the sedimentation method can be explained by Stoke's law, in which soil particles with smaller diameters settle slower than the larger particles. In SA, the gravimetric percentages of clay, silt, and sand particles are 2%, 88%, and 10%, respectively (Fig. 4). On the other hand, SC was prepared by mixing SB with the eliminated clay particles obtained during the preparation of SA. As shown in Fig. 4, SC consists of 35% clay, 64% silt, and 1% sand. It is clear that, although all the three tested soils are obtained from the same loess collected in situ, they contain different amounts of clay particles. Additional physical properties of SA, SB, and SC are summarized in Table 1.

Table 2 shows the measured mineral component of SA, SB, and SC obtained through XRD tests. The XRD test was carried out with the Bruker/Siemens D5000 automated diffractometer. The Cu Kα radiation has an excitation energy of 40 kV and 30 mA, a step of 0.02°, a scan speed of 0.02° per 2 s, and diffraction angles of 2°–42°. The software Materials Data Jade 9.3.3 was utilized to analyze the peaks in the diffraction pattern to identify the clay and non-clay minerals. Both non-clay minerals (i.e. quartz, anorthite, calcite, and potassium feldspar) and clay minerals (i.e. illite, chlorite, kaolinite, smectite, and interstratified illite-smectite) are identified in the tested soils. SA, SB, and SC contain 89.9%, 76.2%, and 65.7% non-clay minerals, respectively, indicating that non-clay minerals dominate the composition of the tested soils. Furthermore, the total amount of clay minerals contained in SA, SB, and SC are 7.0%, 23.3%, and 32.9%, respectively. Comparisons of the measured results of soil compositions in SA, SB, and SC confirm that the contents of clay minerals in SA and SC were successfully reduced and enhanced through the sedimentation method, respectively. It should be noted that the retained 7% of clay minerals in SA is attributed to the clay particles sticking firmly to the surface of silt particles and settling in parallel with the silt particles (see the following analysis on Fig. 6a).

4 Specimen preparation method

The method for the preparation of reconstituted specimens proposed by Burland (1990) was utilized to prepare soil specimens with SA, SB, and SC. The soils were first air-dried and then mixed with tap water to a water content of 1.5 times the liquid limit. The consolidation was conducted with the slurry in an oedometer cell through the application of an effective normal stress of 50 kPa. Soil specimens were finally acquired by pushing the invar ring into the oedometer cell. Both the tops and bottoms of the soil specimens were smoothed through a cutter. Four soil specimens of SB and one soil specimen for each of SA and SC were prepared for the following tests.

5 Test program

Two series of tests were conducted with SA, SB, and SC using the thermal invar oedometer. The objective of the first test series (i.e. SA50, SB50, and SC50) (Table 3) is to investigate the role of clay particles in the thermal volumetric behavior of loess. To meet this objective, the axial strains of SA, SB, and SC under heating-cooling cycles were measured and compared. The effective normal stress applied to each of the soil specimens was 50 kPa. In addition to the clay content, the void ratios of SA, SB, and SC are also different at the same effective normal stress (Table 3). At the effective normal stress of 50 kPa, SA50 has a 25% and a 52% smaller void ratio than that of SB50 and SC50, respectively (Table 3).

To interpret the experimental results of the first test series, the influence of the soil void ratio on the thermally induced axial strain of loess was investigated in the second test series. Heating-cooling cycles were applied to three specimens of SB (i.e. SB50, SB100, and SB200) under different effective normal stresses (i.e. 50 kPa, 100 kPa, and 200 kPa). Prior to the cyclic heating-cooling, the void ratios of SB50, SB100, and SB200 were 0.822, 0.750, and 0.681, respectively. Details of the test program and state parameters of each soil specimen are summarized in Table 3.

6 Test procedure

Fig. 5 shows the stress path of all thermal oedometer tests carried out in this study. The soil specimen was placed into the oedometer cell and then water was slowly infiltrated into the cell. The soil specimen was submerged and saturated for 24 h at a condition of zero external stress. It should be noted that a vacuum of 80 kPa was applied in the oedometer cell for approximately 24 h during the saturation. The predefined value of the effective vertical stress (i.e. 50 kPa, 100 kPa, and 200 kPa) was applied to the soil specimen by adding deadweight on the loading frame (A0→B0, A0→C0, and A0→D0). During the soil consolidation, the valves (Fig. 2) were open to dissipate the excess pore water pressure (Cui et al., 2017). The soil consolidation was completed when the rate of volume change was smaller than 0.025%/d (Romero et al., 2003). It was found that 44 h was sufficient for the soil consolidation. The effective normal stress selected in this study (i.e. 50 kPa, 100 kPa, and 200 kPa) was beyond the soil pre-consolidation pressures (50 kPa); therefore, the soil specimens were normally consolidated before the application of the heating-cooling cycles.

After consolidation, the specimens were subjected to heating-cooling cycles under drained conditions (B0→B1→B0, C0→C1→C0, and D0→D1→ D0). During heating, the soil temperature was increased from 25 °C to 65 °C with an interval of 10 °C. Subsequently, the soil specimen was cooled from 65 °C to 25 °C in steps of 20 °C. At each heating/cooling step, the cut-off criterion of thermal equalization was based on the axial strain rate, i.e. smaller than 0.025%/d (Romero et al., 2003). Based on trial tests, it was found that 5 h was sufficient for thermal equalization for each of the heating and cooling stages. A cyclic heating-cooling test was stopped when the irreversible axial strain during a heating-cooling cycle was smaller than 0.025%. This cut-off criterion for the thermal test was consistent with the measurement accuracy of the strain gauge used in this study (i.e. ±0.025%). Following this criterion, the soil specimens were subjected to three to five heating-cooling cycles.

7 Interpretations of test results

7.1 Microstructural analysis of test soils

Fig. 6a shows an SEM photograph of SA with 800× magnification. Silt particles with a diameter of a few tens of micrometers can be clearly identified in the photograph. More importantly, a small number of clay particles stick firmly to the silt grain surface. It is clear that the soil skeleton of SA is dominated by silt particles. Fig. 6b shows an SEM photograph of SB with 800× magnification. The overall image is quite different from that of SA. A homogeneous soil fabric can be seen in the SEM photograph. Both individual clay and silt particles can be observed. Furthermore, the spaces between silt particles are filled with clay particles. These observations suggest that the clay particles play a significant role in forming the soil skeleton of SB. Similar results were obtained by Liu Z et al. (2016) for their SEM tests of loess in which the clay and silt contents were 19.4% and 77.0%, respectively. The SEM photograph of their specimen showed that the clay particles occupied a 145% larger area than did the silt particles. Fig. 6c shows the SEM photograph of SC with 800× magnification. In contrast to SA and SB, individual silt particles cannot be observed in the SEM photograph. Clay particles either cover the surface of the silt particles or fill in the spaces between silt particles. It is clear that the soil skeleton of SC is dominated by clay particles. Comparisons of SA, SB, and SC show that clay particles play a progressively important role in forming the soil skeleton because of the deliberate specimen preparation method used in this study.

7.2 Volumetric behavior of soils under heating-cooling cycles

Fig. 7 shows the evolution in the axial strain of SA50, SB50, and SC50 with time during the first heating-cooling cycle. At each heating stage, the axial strain of SA increases nonlinearly with time and reaches a plateau after approximately 4 h. The soil volume change can be attributed to the reconfiguration of the soil structure and the excessive pore water pressure generated by heating (Campanella and Mitchell, 1968; Delage et al., 2000). These two processes have opposite effects on the soil volume change that are heating rate dependent (i.e. plastic contraction for the reconfiguration of soil structure and elastic expansion for excessive pore water pressure). It should be noted that the pore water was allowed to drain from the top porous stone during the tests (Fig. 2). Therefore, the final soil volume change would not have been affected by the heating rate because the excessive pore water pressure was completely dissipated. On the other hand, the axial strain of SA increases slightly (i.e. less than 0.03%) with time at each cooling stage, corresponding to an essentially elastic contraction (Hueckel and Baldi, 1990; Zhou and Ng, 2018). For SB and SC, the changes in axial strain with time show a similar pattern to that of SA. More importantly, the thermally induced axial strains of SC, SB, and SA increase progressively at the stable state of each heating-cooling stage.

Fig. 8a shows the thermally induced axial strain of the SA50 specimen at an effective normal stress of 50 kPa during heating-cooling cycles. For the first heating process, the soil specimen contracts with an axial strain of 0.17%. As previously discussed, the soil contraction has been recognized as thermo-plastic collapse (Campanella and Mitchell, 1968). During the subsequent cooling process, a very small amount of contractive axial strain (<0.03%) is induced,

corresponding to an essentially thermo-elastic behavior (Hueckel and Baldi, 1990; Zhou and Ng, 2018). The plastic axial strain accumulates with the increasing number of heating-cooling cycles. In addition, the soil response reaches a stable state after three heating-cooling cycles. In the stable state, almost all thermal strains are reversible. A similar pattern of thermal plastic axial strain of soil was observed in previous studies (Di Donna and Laloui, 2015; Vega and McCartney, 2015; Ng et al., 2019a).

Figs. 8b and 8c show the thermally induced axial strains of SB and SC at an effective normal stress of 50 kPa, respectively. Some similarities and differences were observed in the volume changes among SA, SB, and SC under heating-cooling cycles. The measured soil volumetric behavior of SB and SC showed a similar pattern to that exhibited by SA in which the soil contraction accumulates with increasing numbers of heating-cooling cycles. In contrast, SB reaches a stable state after four heating-cooling cycles, which is slower than for SA whose thermal stabilization is reached after three heating-cooling cycles. For SC, five heating-cooling cycles are applied before the thermal strain reaches a stable state. In addition, the thermal axial strain of SA is smaller than that of SB and SC at a given heating-cooling cycle. To quantitatively analyze the soil deformation behavior under heating-cooling cycles, two parameters are considered and used in this study. The plastic axial strain at a given heating-cooling cycle was used as the first parameter. The other parameter is the linear thermal expansion coefficient that is calculated from the measurements taken during the cooling process at the stable state. Detailed discussions on the plastic axial strain and linear thermal expansion coefficient are given in the following sections.

7.3 Plastic axial strain under heating-cooling cycles

Fig. 9 shows the accumulated plastic axial strains of SA50, SB50, and SC50 with increasing numbers of heating-cooling cycles. The measurements of the reconstituted loess from Ng et al. (2019a) and the silty clay from Di Donna and Laloui (2015) are also plotted for cross-comparisons. The soil specimens tested by Ng et al. (2019a) and Di Donna and Laloui (2015) were normally consolidated under saturated conditions. At the end of the first heating-cooling cycle, the SC50 specimen shows a plastic axial strain of 0.59%, which is 211% and 48% larger than that of the SA50 specimen (axial strain: 0.19%) and SB50 specimen (axial strain: 0.40%), respectively. Furthermore, the differences in the plastic axial strain among these soils increase with the increasing number of heating-cooling cycles. At the final heating-cooling cycle, SA, SB, and SC show very small contractive plastic axial strains (i.e. <0.025%). After several heating-cooling cycles, the soil structure probably reaches a stable state. Therefore, there is negligible reconfiguration of the soil structure and hence contraction during the final heating-cooling cycle. In the stable state, the plastic axial strain of the SC50 specimen is 1.02%, which is 264% and 52% larger than that of the SA50 specimen (axial strain: 0.28%) and SB50 specimen (axial strain: 0.67%), respectively. The differences in the plastic axial strain among these three soils can possibly be attributed to the different clay contents (with 2%, 13%, and 35% clay contents for SA, SB, and SC, respectively). As revealed in the XRD results (Table 2), the clay minerals in the tested loess mainly include kaolinite, chlorite, and illite while the component of silt is dominated by quartz. According to previous studies (Abuel-Naga et al., 2007; Vega and

8

McCartney, 2015; Cui et al., 2016; Ng et al., 2016), the clay minerals (i.e. kaolinite, illite, and chlorite) are more sensitive to thermal fluctuations than quartz because of the electrical double layer. Therefore, the thermally induced axial strain of SC, whose clay content is deliberately enhanced, is larger than those of SB and SA. It should be noted that SA, with only 2% clay compared to 35% clay in SC, has a disproportionally large amount of accumulated plastic strains, i.e. 0.28% for SA compared to 1.02% for SC. Similar results can be observed when comparing the accumulated plastic strain and clay content between SB and SC. This indicates that the thermally induced plastic strain of loess may be also influenced by the reconfiguration of silt (Ng and Zhou, 2014). Further studies are needed to examine the reconfiguration of the structure of silt during heating-cooling cycles. This can be achieved by preparing a soil specimen with no clay particles. In addition, the patterns of the accumulated thermal axial strain of the reconstituted loess (Ng et al., 2019a) and silty clay (Di Donna and Laloui, 2015) are similar to those measurements in this study, albeit with quantitative differences in the plastic axial strain at a given heating-cooling cycle. The different amounts of accumulated axial strains of those soils probably also arise from their different mineral components.

7.4 Linear thermal expansion coefficient

Fig. 10 shows the linear thermal expansion coefficients of SA, SB, and SC at the third, fourth, and fifth cooling processes, respectively. For SA, the accumulated axial strain increases from 0.26% to 0.29% with soil temperature decreasing from 65 °C to 25 °C. The slight increase in accumulated axial strain corresponds to an essentially cooling-induced elastic soil strain (Hueckel and Baldi, 1990; Zhou and Ng, 2018). Because the clay particles have absorbed water (Mu et al., 2018), the thermal contraction of water in the double layer gives rise to the thermal contraction of soil as well as the contraction of the silt particles. Similar contractive strains are observed for SB and SC with decreases in soil temperatures. The linear thermal expansion coefficient of each soil specimen is determined through the linear regression. As shown in Fig. 10, the linear thermal expansion coefficient of SA is 4.4×10^{-6} °C^{-1}, while SB and SC have linear thermal expansion coefficients of 6.1×10^{-6} °C^{-1} and 7.3×10^{-6} °C^{-1}, respectively. The measurements clearly show that SC has a linear thermal expansion coefficient 66% and 20% larger than those of SA and SB, respectively. According to previous studies (Khalili et al., 2010), the soil void ratio has a negligible influence on the soil thermal expansion coefficient once the soil particles exhibit well contacts. On the other hand, clay minerals generally show larger thermal expansion coefficients than non-clay minerals (Campanella and Mitchell, 1968; Vega and McCartney, 2015). Therefore, the larger thermal expansion coefficient of SC can be explained by its larger amount of clay content. Comparing the plastic axial strain and the linear thermal expansion coefficient among SA, SB, and SC confirms that the amount of clay minerals (i.e. kaolinite, chlorite, and illite) has a significant effect on the thermal volume changes in loess. In addition, loess can show different patterns of clay particle distribution based on the specimen preparation methods used (i.e. intact, compacted, and reconstituted). As found by Ng et al. (2019a), reconstituted loess with a clay dominated matrix is more sensitive to temperature changes than compacted and intact loess whose soil skeletons are dominated by silt particles.

7.5 Effects of void ratio on thermally induced volume changes

Fig. 11 shows the measurements of plastic axial strain versus the number of heating-cooling cycles for the SB50, SB100, and SB200 specimens. For all the soil specimens, the plastic axial strain increases up to a certain level with the heating-cooling cycles. At a given heating-cooling cycle, there is no clear trend for the plastic axial strain of SB at different effective normal stress levels. In the stable state, the plastic axial strain of SB at effective normal stresses of 50 kPa, 100 kPa, and 200 kPa are 0.67%, 0.72%, and 0.66%, respectively. These observations show that the soil void ratio has minuscule effects on the thermally induced deformation as long as the specimens have the same over-consolidation ratio value. Similar experimental results were reported by previous researchers focused on clay and silt (Romero et al., 2003; Abuel-Naga et al., 2007). The above test results confirm that the quantitative differences in the plastic contractions among SA, SB, and SC are attributed to their mineral compositions but not the soil void ratio.

8 Conclusions

Based on loess collected in situ, three soils with different clay contents are prepared through the sedimentation method. The soil volumetric behavior under heating-cooling cycles is investigated through a thermal invar oedometer. The interpretation of the test results is primarily focused on the plastic axial strain and linear thermal expansion coefficient. The following conclusions may be obtained:

1. The plastic axial strain of SC is 264% and 52% larger than that of SA and SB, respectively. The linear thermal expansion coefficient of SC is 66% and 20% larger than that of SA and SB, respectively. As revealed from XRD tests, the clay particles in the tested loess are mainly composed of kaolinite, chlorite, and illite, while the component of silt particles is quartz. The clay minerals are more sensitive to temperature variations than quartz. Therefore, SC, whose clay content is deliberately enhanced, exhibits a larger plastic axial strain and linear thermal expansion coefficient than do SA and SB.

2. In the stable state, the plastic axial strains of SB at the effective normal stresses of 50 kPa, 100 kPa, and 200 kPa are 0.67%, 0.72%, and 0.66%, respectively. At the stress range considered in this study, there is no clear trend for the measured plastic axial strain of SB with different pre-consolidation pressures. This indicates that the thermal volume change behavior of loess is independent of the soil void ratio as long as the samples are prepared at the normal consolidate state.

It should be noted that the current study only provides experimental results on the volumetric behavior of loess under cyclic heating-cooling. In a future study, a mathematic model needs to be developed for the general application of the findings in this study.

Contributors

Qing-yi MU, Charles Wang-wai NG, and Chao ZHOU designed the research. Qing-yi MU processed the corresponding data. Qing-yi MU wrote the first draft of the manuscript. Chao

ZHOU and Gordon Gong-dan ZHOU helped to organize the manuscript. Charles Wang-wai NG revised and edited the final version.

Conflict of interest

Qing-yi MU, Charles Wang-wai NG, Chao ZHOU, and Gordon Gong-dan ZHOU declare that they have no conflict of interest.

References

Abuel-Naga HM, Bergado DT, Bouazza A, et al., 2007. Volume change behaviour of saturated clays under drained heating conditions: experimental results and constitutive modeling. *Canadian Geotechnical Journal*, 44(8):942-956.

https://doi.org/10.1139/t07-031

ASTM, 2007. Standard Test Method for Particle-size Analysis of Soils (Withdrawn 2016), ASTM D422-63. National Standards of USA.

ASTM, 2011. Standard Practice for Classification of Soils for Engineering Purposes (Unified Soil Classification System), ASTM D2487-11. National Standards of USA.

Burland JB, 1990. On the compressibility and shear strength of natural clays. *Géotechnique*, 40(3):329-378.

https://doi.org/10.1680/geot.1990.40.3.329

Campanella RG, Mitchell JK, 1968. Influence of temperature variations on soil behavior. *Journal of the Soil Mechanics and Foundations Division*, 94(3):709-734.

Cekerevac C, Laloui L, 2004. Experimental study of thermal effects on the mechanical behaviour of a clay. *International Journal for Numerical and Analytical Methods in Geomechanics*, 28(3):209-228.

https://doi.org/10.1002/nag.332

Cui YF, Nouri A, Chan D, et al., 2016. A new approach to DEM simulation of sand production. *Journal of Petroleum Science and Engineering*, 147:56-67.

https://doi.org/10.1016/j.petrol.2016.05.007

Cui YF, Chan D, Nouri A, 2017. Coupling of solid deformation and pore pressure for undrained deformation—a discrete element method approach. *International Journal for Numerical and Analytical Methods in Geomechanics*, 41(18):1943-1961.

https://doi.org/10.1002/nag.2708

Dach J, Jager J, 1995. Prediction of gas and temperature with the disposal of pretreated residential waste. Proceedings of the 5th International Landfill Symposium, p.665-677.

Delage P, Sultan N, Cui YJ, 2000. On the thermal consolidation of Boom clay. *Canadian Geotechnical Journal*, 37(2):343-354.

https://doi.org/10.1139/t99-105

Di Donna A, Laloui L, 2015. Response of soil subjected to thermal cyclic loading: experimental and constitutive study. *Engineering Geology*, 190:65-76.

https://doi.org/10.1016/j.enggeo.2015.03.003

Hueckel T, Baldi G, 1990. Thermoplasticity of saturated clays: experimental constitutive study. *Journal of Geotechnical Engineering*, 116(12):1778-1796.

https://doi.org/10.1061/(asce)0733-9410(1990)116:12(1778)

Khalili N, Uchaipichat A, Javadi AA, 2010. Skeletal thermal expansion coefficient and thermo-hydro-mechanical constitutive relations for saturated homogeneous porous media. *Mechanics of Materials*, 42(6):593-598.

https://doi.org/10.1016/j.mechmat.2010.04.001

Konrad JM, 1990. Unfrozen water as a function of void ratio in a clayey silt. *Cold Regions Science and Technology*, 18(1):49-55.

https://doi.org/10.1016/0165-232X(90)90037-W

Liu XC, Xu WJ, Zhan LT, et al., 2016. Laboratory and numerical study on an enhanced evaporation process in a loess soil column subjected to heating. *Journal of Zhejiang University-SCIENCE A (Applied Physics & Engineering)*, 17(7):553-564.

https://doi.org/10.1631/jzus.A1600246

Liu Z, Liu FY, Ma FL, et al., 2016. Collapsibility, composition, and microstructure of loess in China. *Canadian Geotechnical Journal*, 53(4):673-686.

https://doi.org/10.1139/cgj-2015-0285

Lu HJ, Li JX, Wang WW, et al., 2015. Cracking and water seepage of Xiashu loess used as landfill cover under wetting-drying cycles. *Environmental Earth Sciences*, 74(11):7441-7450.

https://doi.org/10.1007/s12665-015-4729-4

Mu QY, Ng CWW, Zhou C, et al., 2018. A new model for capturing void ratio-dependent unfrozen water characteristics curves. *Computers and Geotechnics*, 101:95-99.

https://doi.org/10.1016/j.compgeo.2018.04.019

Mu QY, Zhou C, Ng CWW, et al., 2019. Stress effects on the soil freezing characteristic curve under freezing and thawing: equipment development and experimental results. *Vadose Zone Journal*, 18:180199.

Ng CWW, Zhou C, 2014. Cyclic behaviour of an unsaturated silt at various suctions and temperatures. *Géotechnique*, 64(9):709-720.

https://doi.org/10.1680/geot.14.P.015

Ng CWW, Wang SH, Zhou C, 2016. Volume change behaviour of saturated sand under thermal cycles. *Géotechnique Letters*, 6(2):124-131.

https://doi.org/10.1680/jgele.15.00148

Ng CWW, Mu QY, Zhou C, 2017a. Effects of boundary conditions on cyclic thermal strains of clay and sand. *Géotechnique Letters*, 7(1):73-78.

https://doi.org/10.1680/jgele.16.00155

Ng CWW, Mu QY, Zhou C, 2017b. Effects of soil structure on the shear behaviour of an unsaturated loess at different suctions and temperatures. *Canadian Geotechnical Journal*, 54(2):270-279.

https://doi.org/10.1139/cgj-2016-0272

Ng CWW, Mu QY, Zhou C, 2019a. Effects of specimen preparation method on the volume change of clay under cyclic thermal loads. *Géotechnique*, 69(2):146-150.

https://doi.org/10.1680/jgeot.16.P.293

Ng CWW, Chen R, Coo JL, et al., 2019b. A novel vegetated three-layer landfill cover system using recycled construction wastes without geomembrane. *Canadian Geotechnical Journal*, 56(12):1863-1875.

https://doi.org/10.1139/cgj-2017-0728

Romero E, Gens A, Lloret A, 2003. Suction effects on a compacted clay under non-isothermal conditions. *Géotechnique*, 53(1):65-81.

https://doi.org/10.1680/geot.2003.53.1.65

Southen JM, Rowe RK, 2005. Laboratory investigation of geosynthetic clay liner desiccation in a composite liner subjected to thermal gradients. *Journal of Geotechnical and Geoenvironmental Engineering*, 131(7):925-935.

https://doi.org/10.1061/(asce)1090-0241(2005)131:7(925)

Tu XB, Kwong AKL, Dai FC, et al., 2009. Field monitoring of rainfall infiltration in a loess slope and analysis of failure mechanism of rainfall-induced landslides. *Engineering Geology*, 105(1-2):134-150.

https://doi.org/10.1016/j.enggeo.2008.11.011

van Dijk B, 2018. Design of suction foundations. *Journal of Zhejiang University-SCIENCE A (Applied Physics & Engineering)*, 19(8):579-599.

https://doi.org/10.1631/jzus.A1700465

Vega A, McCartney JS, 2015. Cyclic heating effects on thermal volume change of silt. *Environmental Geotechnics*, 2(5):257-268.

https://doi.org/10.1680/envgeo.13.00022

Wang XL, Zhu YP, Huang XF, 2014. Field tests on deformation property of self-weight collapsible loess with large thickness. *International Journal of Geomechanics*, 14(3):04014001.

https://doi.org/10.1061/(ASCE)GM.1943-5622.0000320

Zhan LT, Qiu QW, Xu WJ, et al., 2016. Field measurement of gas permeability of compacted loess used as an earthen final cover for a municipal solid waste landfill. *Journal of Zhejiang University-SCIENCE A (Applied Physics & Engineering)*, 17(7):541-552.

https://doi.org/10.1631/jzus.A1600245

Zhan LT, Li GY, Jiao WG, et al., 2017. Field measurements of water storage capacity in a loess–gravel capillary barrier cover using rainfall simulation tests. *Canadian Geotechnical Journal*, 54(11):1523-1536.

https://doi.org/10.1139/cgj-2016-0298

Zhou C, Ng CWW, 2018. A new thermo-mechanical model for structured soil. *Géotechnique*, 68(12):1109-1115.

https://doi.org/10.1680/jgeot.17.T.031

中文概要

题　目：循环温度荷载下黏粒含量对黄土变形特性的影响

目　的：1. 探讨加热-降温循环温度荷载下黄土中黏土矿物对其变形特性的影响，包括累积塑性压缩变形和热膨胀系数。2. 研究黄土由于施加温度荷载产生变形的微观机理。

创新点： 1. 明确了对黄土由温度荷载引起累积塑性变形具有重要影响的矿物成分；2. 研究得到黄土由于施加温度荷载产生变形的微观机理。
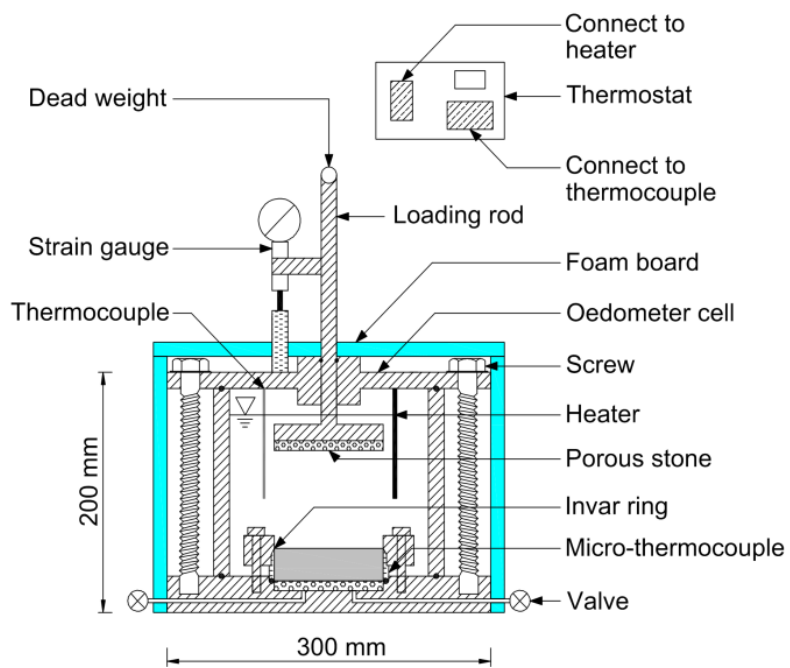
方　法： 1. 通过溶液沉积法，分离黄土中的黏土矿物，并制备出三种不同黏土矿物含量的黄土测试样品；2. 通过温控一维固结仪，测试不同黏土矿物含量的黄土在循环温度荷载下的累积塑性变形和热膨胀系数；3. 通过扫描电镜试验和矿物成分测试，研究黄土由于施加温度荷载产生变形的微观机理。

结　论： 1. 黄土中所含伊利石、绿泥石、高岭石和蒙脱石等黏土矿物对其由于施加温度荷载所产生的累积塑性变形具有重要影响；2. 黄土孔隙比对其由温度荷载引起的累积塑性变形和热膨胀系数影响较小。
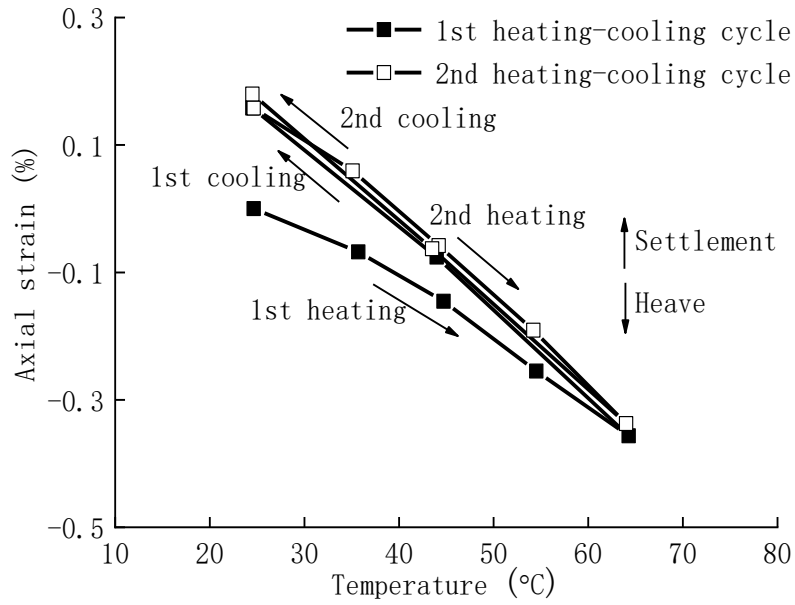
关键词： 黄土；变形；黏土矿物；循环温度荷载
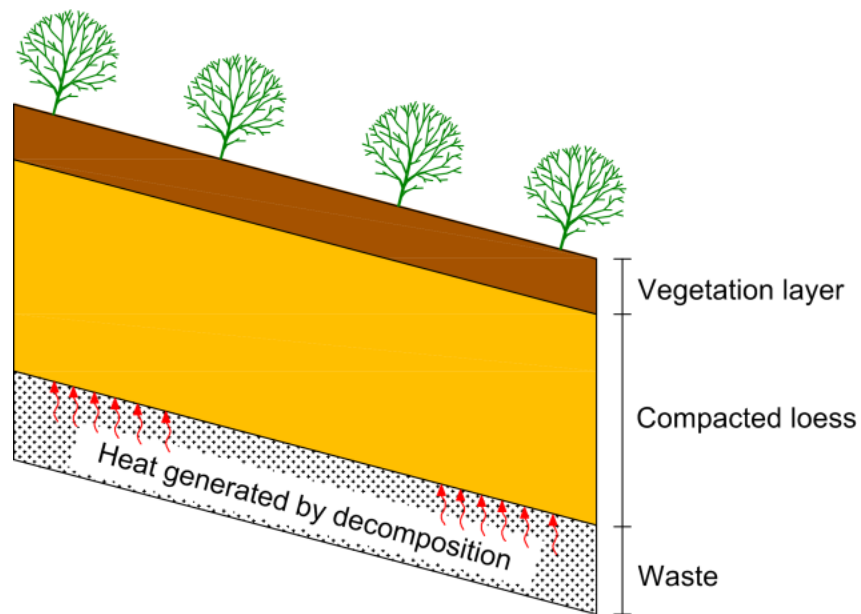
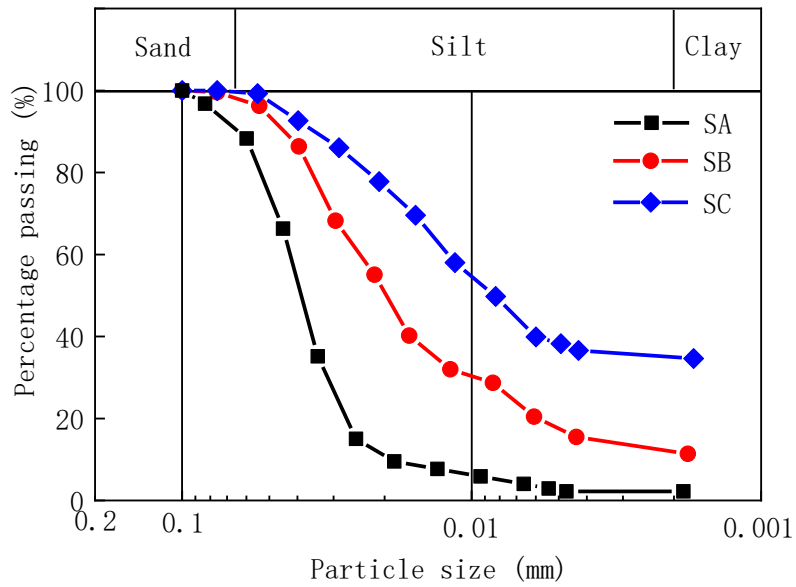**Fig. 1 Illustration of the landfill final cover system used in northwestern China**
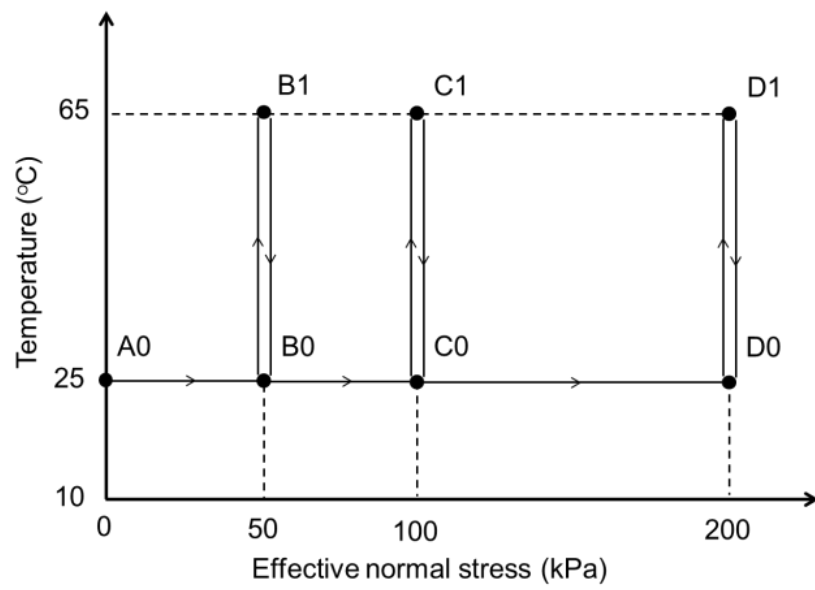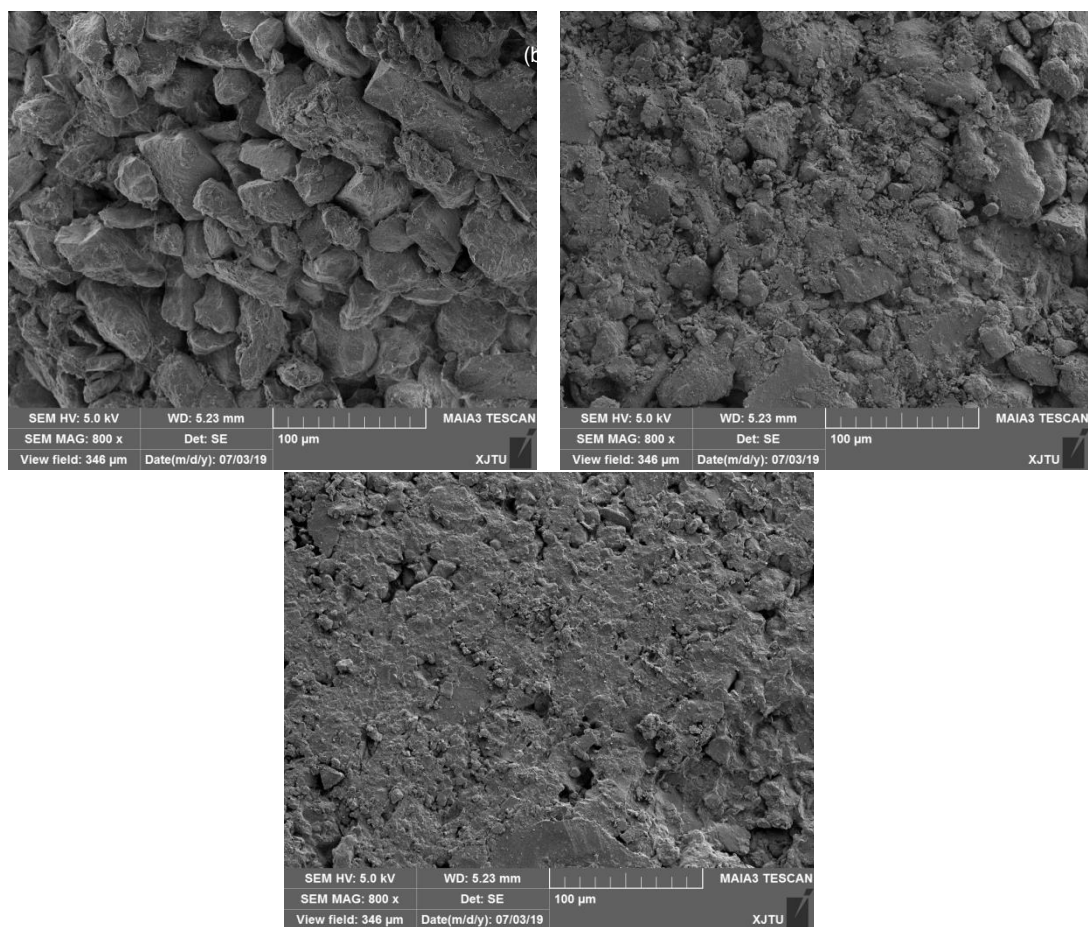

Fig. 2 Illustration of the thermal invar oedometer

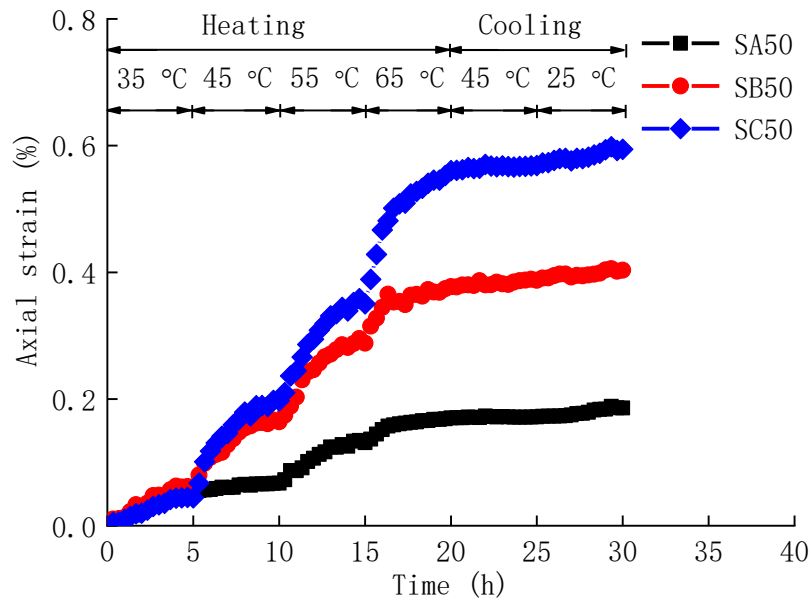**Fig. 3 Calibration of the apparent thermal deformation of the thermal oedometer**

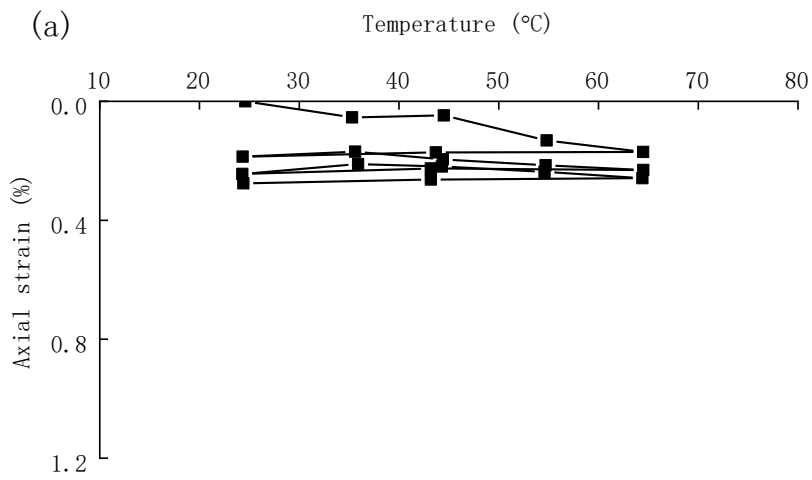**Fig. 4 Particle size distributions of the tested soils**
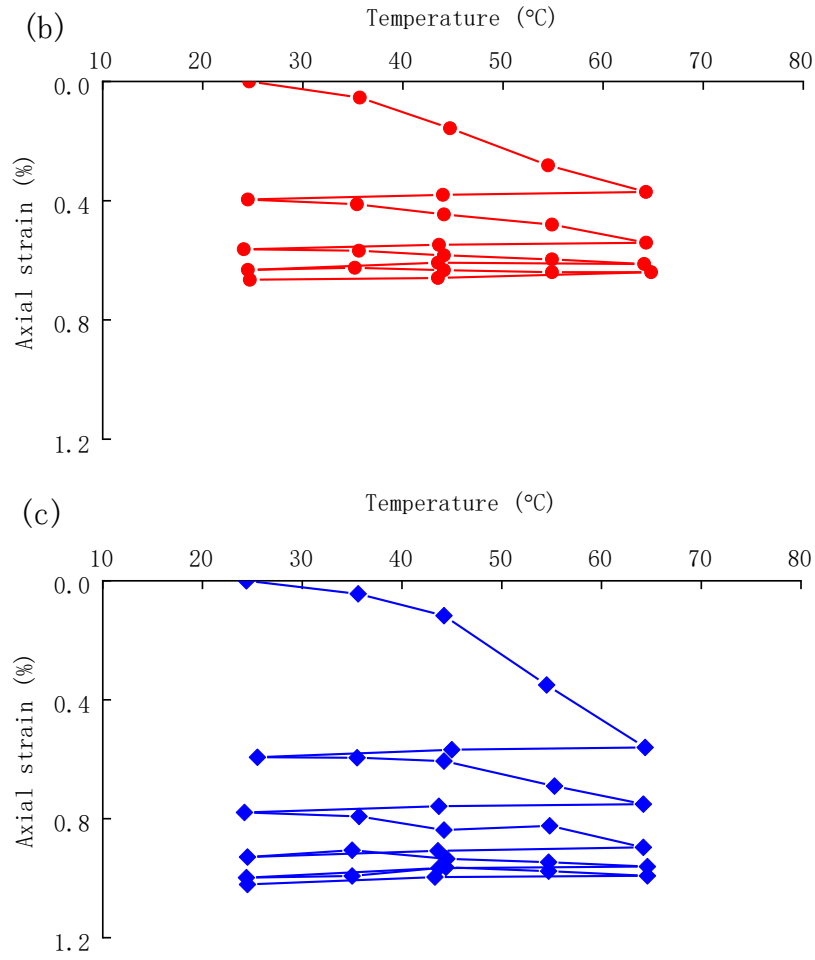
Fig. 5 Stress path of each thermal oedometer test

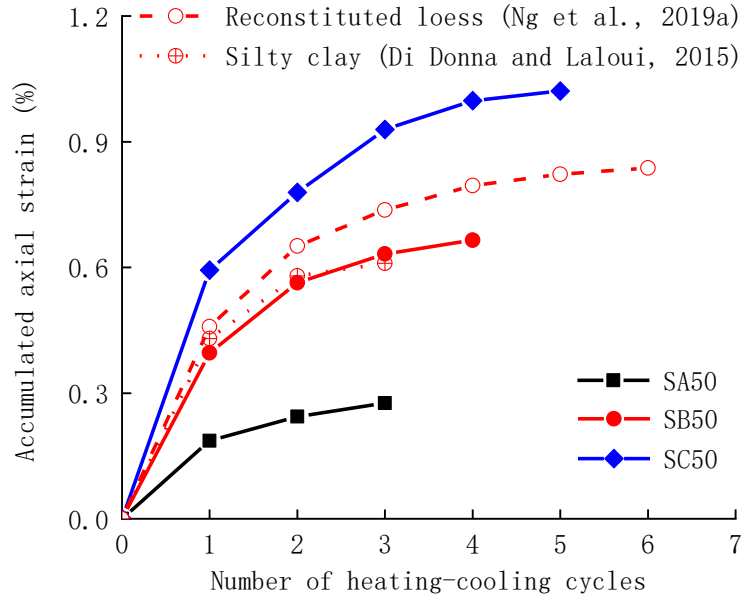**Fig. 6 SEM photographs of SA (a), SB (b), and SC (c)**

Fig. 7 Changes in the axial strain of SA50, SB50, and SC50 with time during the first heating-cooling cycle
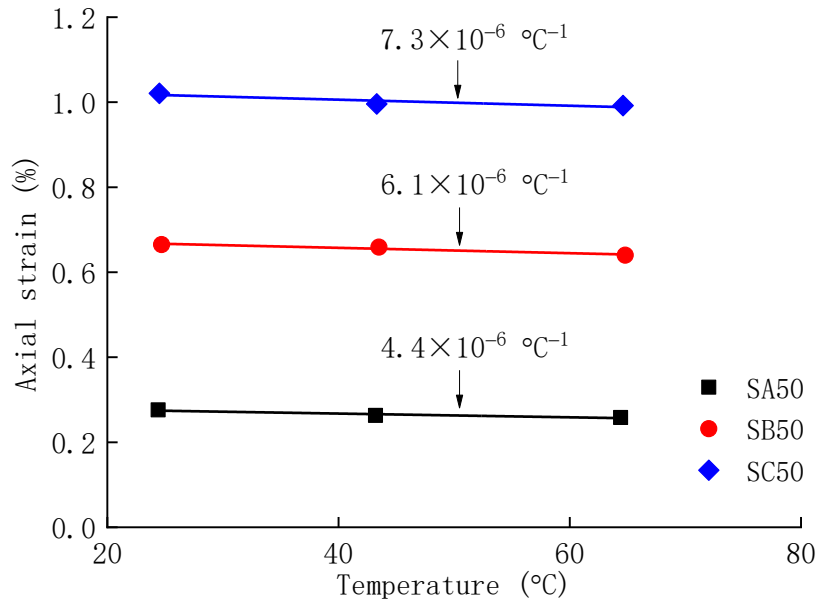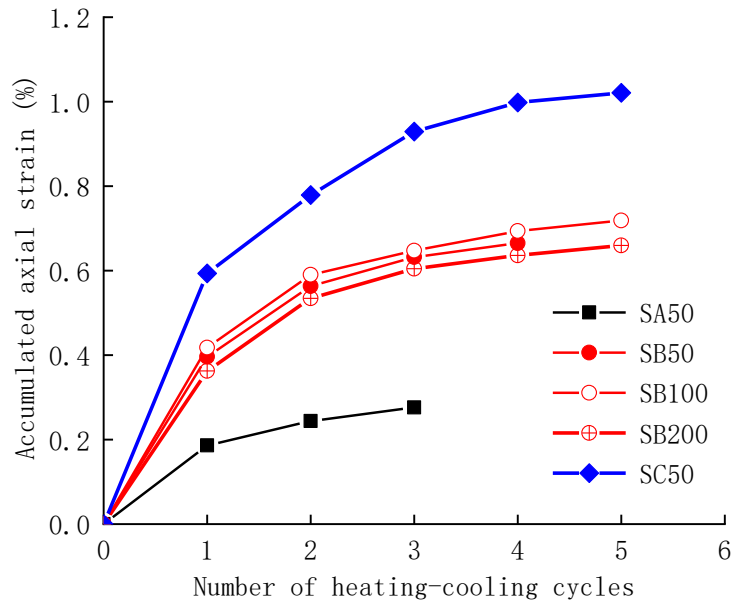

(a)

Fig. 8 Thermally induced axial strains of SA, SB, and SC at an effective normal stress of 50 kPa: (a) SA50; (b) SB50; (c) SC50

Fig. 9 Plastic axial strain of SA, SB, and SC at the effective normal stress of 50 kPa

Fig. 10 Linear thermal expansion coefficients of SA, SB, and SC at the stable state

Fig. 11 Influence of pre-consolidation pressure (void ratio) on the plastic axial strain of SA, SB, and SC at normal consolidation states

Table 1 Physical properties of the tested loess

Parameter	Value		
	SA	SB	SC
Specific gravity	2.67	2.69	2.70
Liquid limit (%)	25	36	45
Plastic limit (%)	12	16	21
Particle size distribution			
Sand (0.063–2 mm) (%)	10	2	1
Silt (0.002–0.063 mm) (%)	88	85	64
Clay (≤0.002 mm) (%)	2	13	35

Table 2 Mineral components of the tested soils

Soil type	Mineral	Component (%)		
		SA	SB	SC
Non-clay mineral	Quartz	49.4	48.1	35.0
	Anorthite	24.7	10.5	12.8
	Calcite	5.4	15.6	15.6
	Potassium feldspar	10.4	2.0	2.3
	Sub-total	89.9	76.2	65.7
Clay mineral	Illite	4.1	14.8	23.7
	Chlorite	1.1	3.5	5.9
	Kaolinite	1.1	3.0	–
	Smectite	–	1.0	–
	Interstratified illite-smectite	0.7	1.0	3.3
	Sub-total	7.0	23.3	32.9

Table 3 Test program and soil states in each test

Soil	Test No.	Initial state		Mechanical loading		Thermal loading	
		e	p_d	e	p_d	e	p_d
SA	SA50	1.001	1.334	0.655	1.613	0.650	1.618
SB	SB50	1.453	1.097	0.822	1.476	0.810	1.486
SC	SC50	1.823	0.956	0.995	1.353	0.975	1.367
SB	SB100	1.453	1.097	0.750	1.537	0.737	1.549
SB	SB200	1.453	1.097	0.681	1.601	0.670	1.611

Note: e is the void ratio; p_d is the dry density (g/cm^3)